Dynamical (e,2e) studies of tetrahydrofurfuryl alcohol

S. M. Bellm,[1,a)] J. D. Builth-Williams,[1] D. B. Jones,[1] Hari Chaluvadi,[2] D. H. Madison,[2] C. G. Ning,[3] F. Wang,[4] X. G. Ma,[4] B. Lohmann,[5] and M. J. Brunger[1,6,b)]
[1]*ARC Centre of Excellence for Antimatter-Matter Studies, Flinders University, GPO Box 2100, Adelaide, South Australia 5001, Australia*
[2]*Department of Physics, Missouri University of Science and Technology, Rolla, Missouri 65409, USA*
[3]*Department of Physics and State Key Laboratory of Low-Dimensional Quantum Physics, Tsinghua University, Beijing 100084, China*
[4]*eChemistry Laboratory, Faculty of Life and Social Science, Swinburne University of Technology, P.O. Box 218, Hawthorn, Melbourne, Victoria 3122, Australia*
[5]*University of the Sunshine Coast, Maroochydore DC, Queensland 4558, Australia*
[6]*Institute of Mathematical Sciences, University of Malaya, 50603 Kuala Lumpur, Malaysia*

(Received 26 April 2012; accepted 31 May 2012; published online 22 June 2012)

Cross section data for electron scattering from DNA are important for modelling radiation damage in biological systems. Triply differential cross sections for the electron impact ionization of the highest occupied outer valence orbital of tetrahydrofurfuryl alcohol, which can be considered as an analogue to the deoxyribose backbone molecule in DNA, have been measured using the (e,2e) technique. The measurements have been performed with coplanar asymmetric kinematics at an incident electron energy of 250 eV, an ejected electron energy of 20 eV, and at scattered electron angles of -5°, -10°, and -15°. Experimental results are compared with corresponding theoretical calculations performed using the molecular 3-body distorted wave model. Some important differences are observed between the experiment and calculations. © *2012 American Institute of Physics*. [http://dx.doi.org/10.1063/1.4729466]

I. INTRODUCTION

In recent years, extensive research has been undertaken into the study of radiation damage in biomolecular systems.[1,2] Monte Carlo track structure simulations are a useful tool to map the path along which primary and secondary species travel as they pass through a biological medium. Such simulations call for a complete set of differential cross sections for both the primary particles and target materials and the secondary particles that are generated. Most track structure simulations focus on water[3,4] as it is the predominant species in living organisms. However, in order to describe the process in a more complete way, the contribution from other species present should also be included in these models.[5]

The data obtained by experimentally measuring selected cross sections provide an important means of testing the theoretical calculations which are used to derive the extensive cross section data needed as input in radiation damage models. In the (e,2e) technique, a projectile electron with well-defined energy and momentum ionizes an atomic or molecular target. The scattered projectile and ejected target electrons are detected in time coincidence with their energies and momenta being determined. The true coincident count rate then yields a multiple differential cross section termed the triple differential cross section (TDCS). Depending on the kinematics employed, the method can be used to determine information about the ionization dynamics of the atomic and molecular targets[6] as well as to reveal details about the bound electronic structure of the target. In the latter case, the kinematics are usually known as electron momentum spectroscopy.[7] Both theoretical and experimental dynamical (e,2e) studies on molecules are comparatively scarce, as a result of some of the considerable challenges involved. For theory these include the description of a multi-centered target, and for experiment the difficulties in resolving different molecular states which are often very closely spaced in energy. We note that while measuring cross sections for isolated molecules in the gas phase, as in the present measurements, can only approximate what occurs in biological systems, it has nonetheless been shown to be a useful initial approach.[8–10]

The sugar deoxyribose is an important molecule in biomolecular systems. Indeed, the sugar-phosphate backbone which is the major structural component in DNA is formed by alternating deoxyribose sugar and phosphate groups as is shown schematically in Figure 1. Thus, largely due to the biological significance of deoxyribose, a number of studies have been undertaken to investigate electron interactions with the deoxyribose analogue molecules: tetrahydrofuran (THF), tetrahydrofurfuryl alcohol (THFA), and 3-hydroxytetrahydrofuran (3HTHF). These include measurements of elastic DCSs for THF,[11–14] THFA,[15] and 3HTHF.[16,17] Total cross sections for electron and positron scattering from THF,[18–20] 3HTHF,[21] and THFA (Refs. 22 and 23) have also been measured. Triple differential cross sections, however, provide the most complete information about the details of the ionization of atomic and molecular targets, which is essential to modelling the deposition of energy in biological matter. Triple differential cross sections have

a)Author to whom correspondence should be addressed. Electronic mail: susan.bellm@flinders.edu.au.
b)Author to whom correspondence should be addressed. Electronic mail: michael.brunger@flinders.edu.au.

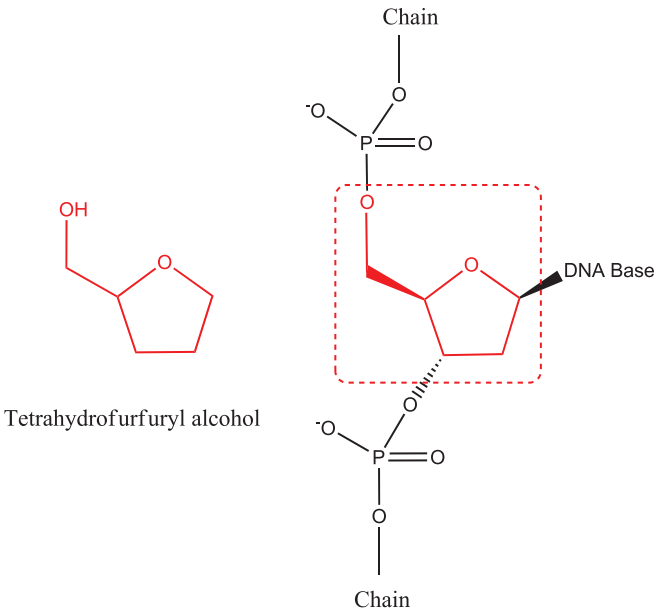

FIG. 1. The structure of the THFA molecule and a segment of the sugar-phosphate backbone of a single strand of DNA.

recently been measured for THF using the (e,2e) technique.[24] To the best of our knowledge the present data are, however, the first TDCSs reported for electron impact ionization of THFA.

The structure of the paper is as follows. In Sec. II, we describe our experimental apparatus and measurement techniques. Thereafter, in Sec. III, some details pertaining to the current theoretical computations are provided. In Sec. IV, we present our results and a discussion of those results, before some conclusions from the present investigations are drawn.

II. EXPERIMENTAL APPARATUS

Triple differential cross section measurements were performed in a coplanar asymmetric geometry using a conventional coincidence spectrometer. As the experimental apparatus has been described in detail in Refs. 24 and 25, only a brief description will be provided here.

Electrons are produced by thermionic emission from a tungsten filament. Five cylindrical electrostatic lens elements are used to collimate and transport the electrons to the interaction region. The resulting electron beam energy resolution is ~0.5 eV (FWHM). The electron beam then crosses a molecular target beam formed by the effusion of THFA molecules through a 0.7 mm internal diameter stainless steel capillary.

Tetrahydrofurfuryl alcohol is a liquid with a relatively low vapour pressure at room temperature; however, it still has sufficient vapour pressure to perform our measurements without directly heating the sample. The THFA sample 99% (Sigma-Aldrich, Australia) was treated with several freeze-pump-thaw cycles prior to use to remove absorbed gases. To prevent possible condensation of THFA within the sample lines, which may contribute to instability in the rate of flow of the sample into the vacuum chamber, the sample lines and vacuum chamber were heated to ~40 °C throughout the measurements.

For the present measurements, the gas capillary and hence the molecular target beam is oriented perpendicular to the scattering plane, which is defined by the momentum vectors of the incident and measured outgoing electrons. The higher energy (scattered) and lower energy (ejected) outgoing electrons are both detected in hemispherical electron energy analyzers, each comprising a 5-element electrostatic entrance lens system, hemispherical selector, and channel electron multiplier detector. The two electron energy analyzers are mounted on independently rotatable turntables concentric with the interaction region. Coincidence timing procedures[26] are used to identify, from the relative arrival times of the electrons at the two detectors, if the two detected electrons are correlated and originate from the same scattering event. Random coincident background events are subtracted using standard statistical methods. The detection energies of the hemispherical electron energy analyzers have been calibrated using the $L_{2,3}M_{2,3}M_{2,3}$ Auger spectrum of argon,[27] while the angular calibration of the analyzers has been determined using the well-defined minimum in the differential cross section for elastic scattering of 60 eV electrons from argon.[28]

In dynamical TDCS measurements, the scattered electron is detected at a fixed forward scattering angle (θ_a) with respect to the incident electron beam direction, while ejected electron angular distributions are measured by scanning the ejected electron energy analyzer and detecting electrons at a number of different ejected electron angles (θ_b) within the scattering plane. The number of true coincidence events detected at each ejected electron angle is proportional to the TDCS. The experiments were performed at an incident electron energy of 250 eV and an ejected electron energy of 20 eV. The energy of the scattered electron is determined by conservation of energy such that

$$E_i = E_a + E_b + \varepsilon_b, \tag{1}$$

where E_i, E_a, and E_b are the kinetic energies of the incident, scattered, and ejected electrons, respectively, and ε_b is the binding energy of the orbital that is ionized.

The TDCS is represented by

$$\frac{d^5\sigma}{d\Omega_a d\Omega_b dE_b}, \tag{2}$$

and it is a measure of the probability that after ionization of a target species by a projectile with energy E_i and momentum $\mathbf{k}_i$, two electrons will be produced with energies E_a and E_b and momenta $\mathbf{k}_a$ and $\mathbf{k}_b$ into the solid angles Ω_a and Ω_b. The momentum transferred to the target is

$$\mathbf{K} = \mathbf{k}_i - \mathbf{k}_a. \tag{3}$$

To establish that the instrument was functioning correctly, the TDCS for the ionization of the helium 1*s* orbital was measured and compared to convergent close coupling calculations under the same kinematics,[29] which are known to produce accurate results.

III. THEORETICAL FRAMEWORK

A. Valence ionization energies and momentum profiles

Quantum mechanical calculations have been undertaken for the valence ionization potentials and momentum profile of the highest occupied molecular orbital (HOMO) of THFA. The chemical structure of THFA is indicated in Fig. 1. Geometry optimizations were performed using the hybrid density functional theory (DFT) model of B3LYP/DGTZVP.[30,31] The DGTZVP basis set of Godbout *et al.*[32] has been proven to be a good basis set for orbital momentum distribution calculations,[33] which can also be applied to larger molecules.[34] The ionization potential energies of THFA are calculated using the outer valence Green function OVGF/DGTZVP model. The *i*th momentum-space wave function $\Phi_i(\boldsymbol{p})$ of THFA is produced according to the Dirac transformation theory,[30] in which the *i*th molecular orbital can be transformed from the coordinate space representation

$$\Phi_i(\boldsymbol{p}) = (2\pi)^{-\frac{3}{2}} \int \exp(-i\,\boldsymbol{p}\cdot\boldsymbol{r})\psi_i(\boldsymbol{r})d\boldsymbol{r}. \tag{4}$$

Here, the coordinate space wave function $\psi_i(\boldsymbol{r})$ is obtained within a Kohn-Sham orbital approximation from electronic structure calculations employing the B3LYP/DGTZVP model and using the GAUSSIAN 09 computational chemistry package.[35] The momentum profile $\rho(\boldsymbol{p})$ is then generated by averaging the orbital density over the unknown orientation of the molecule

$$\rho(\boldsymbol{p}) = \int \Phi_i(\boldsymbol{p})^* \Phi_i(\boldsymbol{p}) d\Omega. \tag{5}$$

B. Triple differential cross sections

The molecular 3-body distorted wave (M3DW) approximation has also been presented in previous publications,[36–38] so only a brief outline of the theory will be presented. The TDCS for the M3DW is given by

$$\frac{d^5\sigma}{d\Omega_a d\Omega_b dE_b} = \frac{1}{(2\pi)^5}\frac{k_a k_b}{k_i}(|T_{dir}|^2 + |T_{exc}|^2 + |T_{dir} - T_{exc}|^2), \tag{6}$$

where $\vec{k}_i$, $\vec{k}_a$, and $\vec{k}_b$ are the wave vectors for the initial, scattered, and ejected electrons, T_{dir} is the direct scattering amplitude, and T_{exc} is the exchange amplitude. The direct scattering amplitude is given by

$$T_{dir} = \langle \chi_a^-(\vec{k}_a, \mathbf{r}_1)\chi_b^-(\vec{k}_b, \mathbf{r}_2) C_{scat-eject}(r_{12}^{ave}) \times |V - U_i| \phi_{DY}^{OA}(\mathbf{r}_2)\chi_i^+(\vec{k}_i, \mathbf{r}_1)\rangle. \tag{7}$$

Here, r_1 and r_2 are the coordinates of the incident and the bound electrons, χ_i, χ_a, and χ_b are the distorted waves for the incident, scattered, and ejected electrons, respectively, and $\phi_{DY}^{OA}(r_2)$ is the initial bound-state Dyson molecular orbital averaged over all orientations. Under the frozen orbital approximation, the Dyson orbital can be well approximated using the initial bound Kohn-Sham orbital. The molecular wave functions were calculated using DFT along with the standard hybrid B3LYP (Ref. 31) functional by means of the Amsterdam density functional (ADF 2007) program[39] with the triple-zeta with two polarization functions Slater type basis sets. The factor $C_{scat-eject}(r_{12}^{ave})$ is the Ward-Macek average Coulomb-distortion factor between the two final state electrons,[40] V is the initial state interaction potential between the incident electron and the neutral molecule, and U_i is a spherically symmetric distorting potential which is used to calculate the initial-state distorted wave for the incident electron $\chi_i^+(\vec{k}_i, \mathbf{r}_1)$. For the exchange amplitude T_{exc}, particles 1 and 2 are interchanged in Eq. (7).

The Schrödinger equation for the incoming electron wave function is given by

$$\left(T + U_i - \frac{k_i^2}{2}\right)\chi_i^+(\vec{k}_i, r) = 0, \tag{8}$$

where T is the kinetic energy operator and the "+" superscript on $\chi_i^+(\vec{k}_i, r)$ indicates outgoing wave boundary conditions. The initial state distorting potential contains three components $U_i = U_s + U_E + U_{CP}$, where U_s contains the nuclear contribution plus a spherically symmetric approximation for the interaction between the projectile electron and the target electrons which is obtained from the quantum mechanical charge density of the target. The charge density is obtained by summing 2 $|\phi_{DY}|^2$ over all occupied orbitals (the 2 is for double occupancy and the original non-averaged Dyson orbital is used). The nuclear contribution to U_s is the interaction between the projectile electron and all the 17 nuclei averaged over all orientations. Averaging the nuclei over all orientations is equivalent to putting the nuclear charge on a thin spherical shell whose radius is the distance of the nuclei from the center of mass (CM). For THFA, there is no nucleus at the CM and the closest nucleus to the CM is a carbon at 1.15 a_0 from the CM. Consequently, the first nuclear sphere has a charge of 6 with a radius of 1.15 a_0. The next sphere is another carbon atom with charge 6 and a radius of 2.24 a_0, while the following sphere is an oxygen atom with charge 8 and a radius of 2.61 a_0. This process continues for the 17 nuclei and the last one is a hydrogen atom with charge 1 and a radius of 6.53 a_0.

U_E is the exchange potential of Furness-McCarthy (corrected for sign errors; Ref. 41) which approximates the effect of the continuum electron exchanging with the passive bound electrons in the molecule, and U_{CP} is the correlation-polarization potential of Perdew and Zunger[42] and Pardial and Norcross.[43]

In Eq. (7), the final state for the system is approximated as a product of distorted waves for the two continuum electrons (χ_a^-, χ_b^-) times the Ward-Macek average Coulomb-distortion factor $C_{scat-eject}$. The final state distorted waves are calculated the same as the initial state except that the final state charge density is used to calculate U_s. The final state charge density is obtained the same as for the initial state except that unity occupancy is used for the active electron orbital. Additional details can be found in Madison and Al-Hagan.[44]

Results are presented for the M3DW described above, as well as the standard distorted wave Born approximation

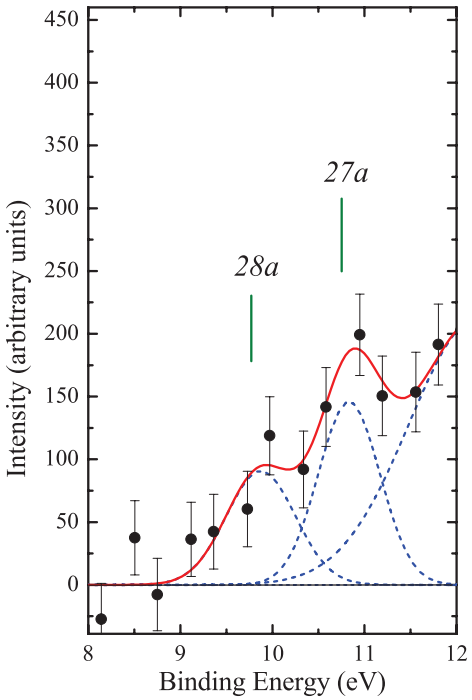

FIG. 2. Measured binding energy spectrum for the outer valence region of THFA showing the HOMO (28a) and NHOMO (27a). The data have been fitted with a sum of Gaussian functions, using a convolution of the coincidence binding energy resolution and the natural line width of the molecular orbitals to define the peak width parameters.

(DWBA). The DWBA is identical to the M3DW except that the post-collision interaction (PCI) term, $C_{scat-eject}(r_{12}^{ave})$, is omitted in the evaluation of the direct and exchange amplitudes.

IV. RESULTS AND DISCUSSION

Figure 2 shows the measured binding energy spectrum for the outer valence region of THFA. The incident electron energy was 250 eV. Ejected electrons were detected at an energy of 20 eV, while the energy of the detected scattered electrons was varied. The scattered and ejected electrons were detected in this case at fixed angles of -10° and 90°, respectively. The instrumental binding energy resolution under the chosen conditions was estimated to be 1.1 eV FWHM, from the width of the helium 1*s* binding energy peak measured under the same kinematics. The binding energy spectrum has been fitted with a sum of three Gaussian functions of fixed widths that represent the contributions of different molecular orbitals. As the instrumental binding energy resolution is comparable to the natural line width of the orbitals observed in photoelectron spectra of THFA,[45] the width of the individual peaks in the Gaussian fitting was determined by adding the coincidence resolution and the respective natural widths of each molecular orbital in quadrature. With our coincidence energy resolution, we are unable to completely resolve the highest occupied molecular orbital from the next highest occupied molecular orbital (NHOMO).

A THFA molecule contains a five membered heterocyclic furanose ring which undergoes pseudorotation. This is an internal motion that involves out-of-plane ring puckering vibrations which occur in a way that makes the phase of the puckering rotate about the ring.[46] Twenty possible conformations of THFA may be produced through pseudorotation in the gas phase.[47] The molecular structure of THFA in the gas phase has been investigated by electron diffraction and *ab initio* methods,[47] which suggested the presence of two conformers with abundances of 84 ± 8% and 16 ± 8%. Hence, in practice the population of our THFA beam is essentially dominated by one conformer. In the most stable conformers, the O–H group is directed toward the ring oxygen and seems to be stabilised by hydrogen bonding.[47]

TABLE I. Ionization energies for the outer valence region of THFA. Calculations have been performed using the OVGF/DGTZVP model. The spectroscopic pole strength for each orbital is given in parentheses. The error in the ionization energy for the present experimental data is ±0.6 eV. The PES data are from Ibanescu *et al.*[45]

Orbital	OVGF/DGTZVP (eV)[a]	Present results (eV)	PES (eV) (Ref. 45)
28a	9.79 (0.91)	9.8	9.81
27a	10.93 (0.91)	10.7	10.60
26a	11.47 (0.91)		
25a	11.86(0.91)		
24a	12.09 (0.91)		
23a	12.41 (0.91)		
22a	13.24 (0.91)		
21a	14.03 (0.91)		
20a	14.37 (0.91)		
19a	14.65 (0.90)		
18a	15.62 (0.91)		
17a	16.39 (0.90)		

Table I shows the calculated ionization potentials for the outer valence orbitals of THFA in the region below 18 eV, together with the present (e,2e) results and values determined from photoelectron spectroscopy (PES) measurements.[45] The calculations have been performed using the OVGF/DGTZVP model. The spectroscopic pole strength (SP) is given in parentheses for each of the outer valence states. In each case, the magnitude of the SP is greater than 0.90 indicating that the independent particle approximation employed is a valid approximation. The calculated IPs of the frontier orbitals, that is the HOMO (28a) and the NHOMO (27a), of THFA are 9.79 eV and 10.93 eV, respectively. This agrees well with the present experimental electron binding energies of 9.8 ± 0.6 eV and 10.7 ± 0.6 eV for the HOMO and NHOMO, respectively. The present measured results are also in good agreement with the appearance energy measured for the THFA parent cation of 9.43 ± 0.12 eV (Ref. 48) and with previous photoelectron spectroscopy measurements.[45]

The calculated momentum density probability distribution for the HOMO of THFA is presented in Figure 3. Usually an s-type orbital (dominated by s-electrons) has an orbital momentum profile with a half bell shape where the momentum profile starts from a maximum and decreases to a minimum, whereas a p-type orbital is represented by a bell-shaped curve. The profile suggests that the HOMO of THFA is predominantly a p-type molecular orbital. Similarly, the NHOMO has significant p-type character. The inset in Fig. 3 shows the

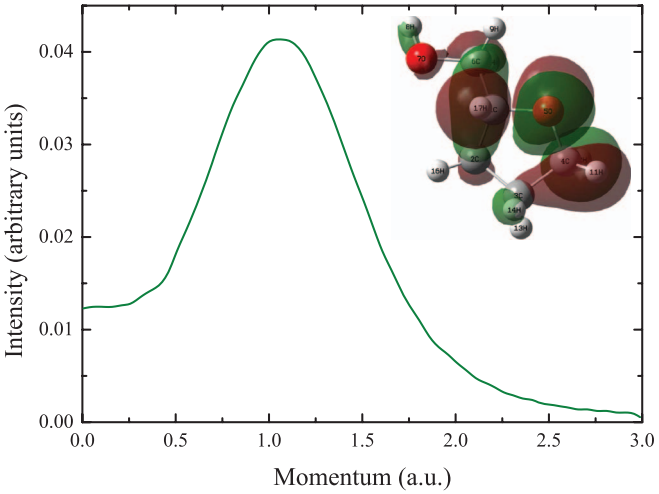

FIG. 3. The momentum density probability distribution for the HOMO of THFA and the molecular orbital electron density distribution for the HOMO (inset).

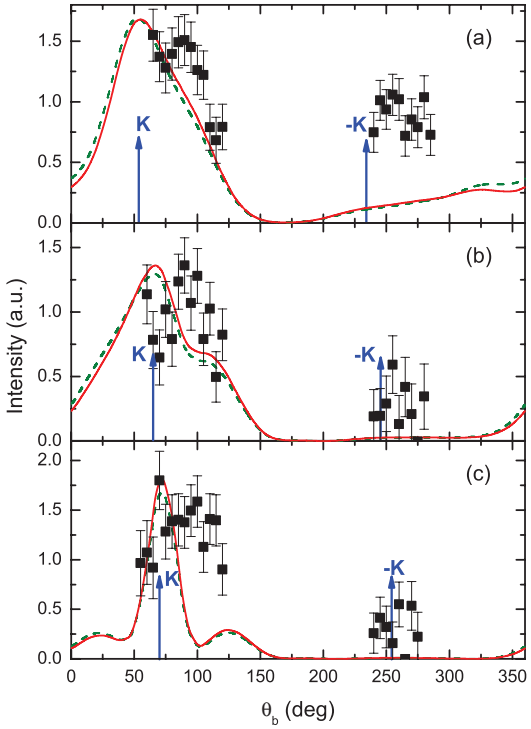

FIG. 4. The triple differential cross sections for ionization of the HOMO of THFA with $E_0 = 250$ eV and $E_b = 20$ eV. The scattered electron detection angles and corresponding momentum transfers are (a) $-5°$, $|K| = 0.45$ a.u., (b) $-10°$, $|K| = 0.77$ a.u., and (c) $-15°$, $|K| = 1.12$ a.u. The positions of the momentum transfer vector, $+\mathbf{K}$, and $-\mathbf{K}$ are indicated by the arrows. Points are the experimental data. Solid curve (red): M3DW calculation for the HOMO. Dashed curve (green): DWBA calculation for the HOMO (see text for details).

orbital electron density distribution for the HOMO (28a) and also indicates that the HOMO of THFA is dominated by out-of-plane contributions of 2*p* electrons from atoms on the ring. Such a p-type orbital would normally lead us to anticipate the binary peak in our TDCS possessing a double lobe structure. However, Figure 3 does suggest a quite significant intensity at small momenta which, if due to some sort of s-p hybridisation, might complicate our interpretation of the situation (see later).

Figures 4(a)–4(c) show the present experimental and theoretical TDCS results for the HOMO of THFA. The relatively large error bars on the experimental data result from the small magnitude of the coincidence cross section. Traditionally, the angular distributions are divided into two regions, the binary region ranging from 0° to 180° and the recoil region which ranges from 180° to 360°. In the binary region, structure is attributed to single binary collisions and depending upon the kinematics, may contain strong signatures of the orbital structure.[49] In contrast, in the recoil region structure arises from processes in which the ejected electron produced by an initial binary collision undergoes subsequent recoil scattering from the target nucleus. The distributions have a binary lobe centered close to the momentum transfer direction ($+\mathbf{K}$) and a recoil lobe pointing in the opposite direction ($-\mathbf{K}$). Coulomb repulsion between the final state electrons causes a shift of the binary peak, to larger scattering angles, away from the momentum transfer direction.

Two theoretical calculations are presented in Fig. 4. The solid line (red) denotes the M3DW calculation and the dashed (green) line the DWBA calculation. As the experimental data are only relative they are attributed absolute values by normalization to the M3DW theory to give the best visual fit in the binary peak region. Measuring absolute TDCS data is not a straightforward process.[50,51] Although a relatively simple method for absolute (e,2e) measurements was recently described in the literature,[51] due to the high density of molecular orbitals here, such measurements would be very difficult to apply to a target like THFA. The main difference between the M3DW and DWBA calculations is that the PCI between the scattered and ejected electrons is not included in the evaluation of the direct and exchange amplitudes in the DWBA calculation. However, there appears very little difference between the two calculations suggesting that the inclusion of PCI in the model is relatively unimportant under these kinematics.

The size of the recoil peak for the scattered electron angles of $-10°$ and $-15°$ in Figs. 4(b) and 4(c) is small, indicating that there is not a large amount of interaction of the ejected electron with the molecular ion. The recoil peak at the scattered electron angle of $-5°$ is somewhat stronger in magnitude, relative to the binary peak, both in the experimental data and theoretical calculations. However, the theory does significantly underestimate the recoil intensity here as well as at both the other scattered electron angles investigated, which is likely due to insufficient nuclear scattering strength being included in the calculations. This is caused by spreading the nuclear charge over a spherical shell when averaging the nuclei over all orientations, resulting in a nuclear interaction that is too weak.

The binary peak in the experimental data shown in Fig. 4(b) for the scattered electron angle of $-10°$ shows the suggestion of a dip in the distribution around the momentum transfer direction. As double peak structures are characteristic of ionization of atomic p-states, the dip in the distribution

suggests that this structure may result from ionization of a p-type orbital. This is consistent with the HOMO being largely a p-type molecular orbital as is indicated by the orbital momentum density probability distribution in Fig. 3. However, the dip is not particularly evident in Fig. 4(c) at the scattered electron angle of -15° where it might be expected to be more pronounced as it is closer to Bethe ridge kinematics. On the Bethe ridge, the kinematics satisfy the requirement that all momentum is transferred to the bound, target electron during the collision and the ion essentially acts as a spectator. We previously suggested that the small recoil peak intensity observed for some molecular targets, in particular CHCOOH and THF, relative to H_2O was due to the lack of a charge center at the molecule's center of mass.[24,52] An alternative explanation has been proposed by Xu *et al.*,[53] which is that rather than being related to the geometry of the target this observation more simply results from the momentum profile of the orbitals investigated and the kinematics being close to the Bethe ridge. Following from this argument, as a consequence of the momentum profile of the HOMO of THFA having non-zero intensity at zero momentum (see Fig. 3), in the region of the Bethe ridge the recoil peak intensity should be relatively small. This is similar to the HOMO for CHOOH and THF which also have momentum profiles with significant non-zero intensity at zero momentum.[54,55] In contrast, the very strongly p-like momentum profiles[56] investigated for H_2O exhibit a much larger recoil peak relative to the binary peak.[57]

The M3DW and DWBA calculations show a multi-peaked structure in the binary region in Fig. 4(c), with a narrow binary peak centered close to $+\mathbf{K}$ and two smaller shoulders. The calculated binary peaks in Figs. 4(a) and 4(b), while much broader than that in Fig. 4(c), are still centered close to $+\mathbf{K}$. In contrast, the experimental binary peaks appear shifted to significantly larger ejected electron emission angles. As noted earlier, we are unable to completely resolve the HOMO from the NHOMO so that some inconsistency between theory and experiment may arise from contributions from the NHOMO to the measured TDCS.

The binary peaks in the present experimental measurements appear quite broad, which appears to be characteristic of TDCS measurements for a number of molecular targets. Comparably broad binary peaks have also been observed in experimental studies for molecules including water,[57] formic acid,[52] methane,[58] and nitrogen[59] under similar kinematics. Broad binary peaks were also observed for TDCS measurements of the HOMO of THF.[24] Note that THF and THFA are very similar in structure. Both are five membered heterocyclic ether compounds and in THFA a hydrogen atom on the alpha-carbon is substituted by a CH_2OH group. Interestingly, much narrower binary peaks have been observed both for ionization of the HOMO in pyrimidine[60] and for the inner valence orbitals in thymine,[61] again under similar kinematics. This observation is possibly related to the structure of the molecular rings in pyrimidine and thymine, which are both six membered ring type structures. Pyrimidine belongs to the group of diazines and contains two nitrogen atoms which are located at the meta-positions in the ring and thymine is a pyrimidine derivative.

V. CONCLUSIONS

We have presented experimental and theoretical TDCS measurements for THFA, which is an important analogue molecule for the deoxyribose molecule found in DNA. The measured binding energies are in good agreement with the present quantum chemical calculations and previous PES data. The measured TDCSs at all three scattered electron detection angles investigated exhibit a quite broad binary peak, with only a suggestion for the double-lobed structure we anticipated from a p-type orbital. Although the theoretical width of the binary peak was quite broad and similar to the experimental data for scattered electron detection angles of -5° and -10°, for -15° the theory is significantly narrower than the experimental measurements. The TDCSs at scattered electron detection angles of -15° and -10° showed a small recoil peak relative to the magnitude of the binary peak, indicating that there is very little interaction between the ejected electron and the target ion under these kinematical conditions. In contrast at -5°, there is considerable intensity in the recoil peak. Only a small difference was observed between the M3DW and DWBA calculations, suggesting that post-collision interaction effects were unimportant in the kinematical conditions of this investigation. While our theory indicates that PCI effects are unimportant here, the shift in the binary peak away from $\mathbf{K}$ in our experimental data might suggest that PCI is in fact playing a role in the collision dynamics. Further investigation into this apparent contradiction is needed. The calculations significantly underestimated the recoil peak intensity observed at all scattered electron detection angles studied, which is attributed to spreading of the nuclear charge over a spherical shell leading to a nuclear interaction that is too weak. The calculations performed within the M3DW model were not in good agreement with the experimental data, which is perhaps not surprising given the complexity of the molecular target and the inability to completely resolve the HOMO from the NHOMO in the experimental measurements. Further work is needed to probe the discrepancies highlighted above.

ACKNOWLEDGMENTS

This work was supported by the Australian Research Council Centre of Excellence for Antimatter-Matter Studies, an Australian Research Council Discovery Project grant and by the U.S. National Science Foundation (NSF) under Grant. No. PHY-1068237. The author C.N. would like to acknowledge the support of the National Natural Science Foundation of China (NNSFC) under Contract No. 10704046. One of us (M.J.B.) also thanks the University of Malaya for his "Distinguished Visiting Professor" appointment. F.W. acknowledges the National Computational Infrastructure (NCI) at the Australian National University for an award under the "Merit Allocation Scheme" for supercomputing facilities.

[1] L. Sanche, Eur. Phys. J. D **35**, 367 (2005).
[2] L. Sanche, Mass Spectrom. Rev. **21**, 349 (2002).
[3] A. Munoz, F. Blanco, G. Garcia, P. A. Thorn, M. J. Brunger, J. P. Sullivan, and S. J. Buckman, Int. J. Mass. Spectrom. **277**, 175 (2008).
[4] A. G. Sanz, M. C. Fuss, A. Munoz, F. Blanco, P. Limao-Vieira, M. J. Brunger, S. J. Buckman, and G. Garcia, Int. J. Radiat. Biol. **88**, 71 (2012).

[5]M. U. Bug, W. Y. Baek, and H. Rabus, Int. J. Radiat. Biol. **88**, 137 (2012).
[6]A. Lahmam-Bennani, J. Phys. B **24**, 2401 (1991).
[7]I. E. McCarthy and E. Weigold, Rep. Prog. Phys. **51**, 299 (1988).
[8]S. Ptasinska, S. Denifl, P. Scheier, and T. D. Mark, J. Chem. Phys. **120**, 8505 (2004).
[9]P. Swiderek, Angew. Chem., Int. Ed. **45**, 4056 (2006).
[10]R. D. White and R. E. Robson, Phys. Rev. Lett. **102**, 230602 (2009).
[11]A. R. Milosavljevic, A. Giuliani, D. Sevic, M. J. Hubin-Franskin, and B. P. Marinkovic, Eur. Phys. J. D **35**, 411 (2005).
[12]C. S. Trevisan, A. E. Orel, and T. N. Rescigno, J. Phys. B **39**, L255 (2006).
[13]M. G. P. Homem, R. T. Sugohara, I. P. Sanches, M. T. Lee, and I. Iga, Phys. Rev. A **80**, 032705 (2009).
[14]C. J. Colyer, V. Vizcaino, J. P. Sullivan, M. J. Brunger, and S. J. Buckman, New J. Phys. **9**, 41 (2007).
[15]A. R. Milosavljevic, F. Blanco, D. Sevic, G. Garcia, and B. P. Marinkovic, Eur. Phys. J. D **40**, 107 (2006).
[16]V. Vizcaino, J. Roberts, J. P. Sullivan, M. J. Brunger, S. J. Buckman, C. Winstead, and V. McKoy, New J. Phys. **10**, 053002 (2008).
[17]A. R. Milosavljevic, F. Blanco, J. B. Maljkovic, D. Sevic, G. Garcia, and B. P. Marinkovic, New J. Phys. **10**, 103005 (2008).
[18]A. Zecca, C. Perazzolli, and M. J. Brunger, J. Phys. B **38**, 2079 (2005).
[19]P. Mozejko, E. Ptasinska-Denga, A. Domaracka, and C. Szmytkowski, Phys. Rev. A **74**, 012708 (2006).
[20]M. Fuss, A. Munoz, J. C. Oller, F. Blanco, D. Almeida, P. Limao-Vieira, T. P. D. Do, M. J. Brunger, and G. Garcia, Phys. Rev. A **80**, 052709 (2009).
[21]A. Zecca, L. Chiari, A. Sarkar, and M. J. Brunger, J. Phys. B **41**, 085201 (2008).
[22]P. Mozejko, A. Domaracka, E. Ptasinska-Denga, and C. Smytkowski, Chem. Phys. Lett. **429**, 378 (2006).
[23]A. Zecca, L. Chiari, G. Garcia, F. Blanco, E. Trainotti, and M. J. Brunger, New J. Phys. **13**, 115001 (2011).
[24]C. J. Colyer, S. M. Bellm, B. Lohmann, G. F. Hanne, O. Al-Hagan, D. H. Madison, and C. G. Ning, J. Chem. Phys. **133**, 124302 (2010).
[25]S. J. Cavanagh and B. Lohmann, J. Phys. B **32**, L261 (1999).
[26]E. Weigold and I. E. McCarthy, *Electron Momentum Spectroscopy* (Plenum, New York, 1999).
[27]L. O. Werme, T. Bergmark, and K. Siegbahn, Phys. Scr. **8**, 149 (1973).
[28]R. Panajotovic, D. Filipovic, B. Marinkovic, V. Pejcev, M. Kurepa, and L. Vuskovic, J. Phys. B **30**, 5877 (1997).
[29]I. Bray, personal communication (2011).
[30]A. D. Becke, J. Chem. Phys. **98**, 5648 (1993).
[31]C. Lee, W. Yang, and R. G. Parr, Phys. Rev. B **37**, 785 (1988).
[32]N. Godbout, D. R. Salahub, J. Andzelm, and E. Wimmer, Can. J. Chem. **70**, 560 (1992).
[33]F. Wang, J. Phys. Chem. A **107**, 10199 (2003).
[34]A. Ganesan, F. Wang, and C. Falzon, J. Comput. Chem. **32**, 525 (2011).
[35]M. J. Frisch, G. W. Trucks, H. B. Schlegel *et al.*, GAUSSIAN 09, Revision A.02, Gaussian, Inc., Wallingford, CT, 2009.
[36]J. F. Gao, D. H. Madison, and J. L. Peacher, J. Chem. Phys. **123**, 204314 (2005).
[37]J. F. Gao, D. H. Madison, and J. L. Peacher, Phys. Rev. A **72**, 032721 (2005).
[38]J. F. Gao, J. L. Peacher, and D. H. Madison, J. Chem. Phys. **123**, 204302 (2005).
[39]C. F. Guerra, J. G. Snijders, G. te Velde, and E. J. Baerends, Theor. Chem. Acc. **99**, 391 (1998).
[40]S. J. Ward and J. H. Macek, Phys. Rev. A **49**, 1049 (1994).
[41]J. B. Furness and I. E. McCarthy, J. Phys. B **6**, 2280 (1973).
[42]J. P. Perdew and A. Zunger, Phys. Rev. B **23**, 5048 (1981).
[43]N. T. Padial and D. W. Norcross, Phys. Rev. A **29**, 1742 (1984).
[44]D. H. Madison and O. Al-Hagan, Journal of Atomic, Molecular, and Optical Physics **2010**, 367180 (2010).
[45]B. C. Ibanescu, O. May, A. Monney, and M. Allan, Phys. Chem. Chem. Phys. **9**, 3163 (2007).
[46]D. O. Harris, G. G. Engerholm, C. A. Tolman, A. C. Luntz, R. A. Keller, H. Kim, and W. D. Gwinn, J. Chem. Phys. **50**, 2438 (1969).
[47]K. B. Borisenko, S. Samdal, I. F. Shishkov, and L. V. Vilkov, J. Mol. Struct. **448**, 29 (1998).
[48]A. R. Milosavljevic, J. Kocisek, P. Papp, D. Kubala, B. P. Marinkovic, P. Mach, J. Urban, and S. Matejcik, J. Chem. Phys. **132**, 104308 (2010).
[49]H. Ehrhardt, K. Jung, G. Knoth, and P. Schlemmer, Z. Phys. D **1**, 3 (1986).
[50]A. Lahmam-Bennani, M. Cherid, and A. Duguet, J. Phys. B **20**, 2531 (1987).
[51]L. R. Hargreaves, M. A. Stevenson, and B. Lohmann, Meas. Sci. Technol. **21**, 055112 (2010).
[52]C. J. Colyer, M. A. Stevenson, O. Al-Hagan, D. H. Madison, C. G. Ning, and B. Lohmann, J. Phys. B **42**, 235207 (2009).
[53]S. Xu, X. Ma, S. Yan, and P. Zhang, J. Chem. Phys. **136**, 237101 (2012).
[54]K. L. Nixon, W. D. Lawrance, and M. J. Brunger, Chem. Phys. Lett. **474**, 23 (2009).
[55]C. G. Ning, Y. R. Huang, S. F. Zhang, J. K. Deng, K. Liu, Z. H. Luo, and F. Wang, J. Phys. Chem. A **112**, 11078 (2008).
[56]R. Cambi, G. Ciullo, A. Sgamellotti, C. E. Brion, J. P. D. Cook, I. E. McCarthy, and E. Weigold, Chem. Phys. **91**, 373 (1984).
[57]D. S. Milne-Brownlie, S. J. Cavanagh, B. Lohmann, C. Champion, P. A. Hervieux, and J. Hanssen, Phys. Rev. A **69**, 032701 (2004).
[58]A. Lahmam-Bennani, A. Naja, E. M. S. Casagrande, N. Okumus, C. Dal Cappello, I. Charpentier, and S. Houamer, J. Phys. B **42**, 165201 (2009).
[59]A. Naja, E. M. Staicu-Casagrande, A. Lahmam-Bennani, M. Nekkab, F. Mezdari, B. Joulakian, O. Chuluunbaatar, and D. H. Madison, J. Phys. B **40**, 3775 (2007).
[60]J. D. Builth-Williams, S. M. Bellm, D. B. Jones, H. Chaluvadi, D. H. Madison, C. G. Ning, B. Lohmann, and M. J. Brunger, J. Chem. Phys. **136**, 024304 (2012).
[61]S. M. Bellm, C. J. Colyer, B. Lohmann, and C. Champion, Phys. Rev. A **85**, 022710 (2012).